Proceedings of the ASME 2024
International Mechanical Engineering Congress and Exposition
IMECE2024
November 17-21, 2024, Portland, Oregon, USA

IMECE2024-139666

A COMPUTATIONAL FLUID DYNAMICS MODEL FOR INVESTIGATION OF MATERIAL FLOW IN A PERFUSION BIOREACTOR TOWARD OPTIMAL BIOMEDICAL DESIGN OF CELL-LADEN SCAFFOLDS FOR BONE REGENERATION

Hannah Rollins
Department of Biomedical Engineering
Marshall University,
Huntington, WV 25755, USA

Roozbeh "Ross" Salary *
Department of Mechanical & Industrial Engineering
Department of Biomedical Engineering
Marshall University,
Huntington, WV 25755, USA

ABSTRACT

In tissue engineering, once a scaffold has completed mechanical property testing, it must then undergo biological characterization which determines if the scaffold is capable of supporting cell viability. To perform biological tests, cells must be seeded onto a scaffold with the help of bioreactors, the four main types being: (i) rotating wall, (ii) spinner flask, (iii) compression, and (iv) perfusion bioreactor. In perfusion bioreactors, a consistent flow of material is introduced (using a pump) into the inlet of the bioreactor chamber where multiple scaffolds of a disc geometry are located. However, the intrinsic, complex interaction between the scaffolds and material flow as it goes through the bioreactor chamber affects the viability of the seeded stem cells. Therefore, there is a need to identify consequential fluid dynamics phenomena governing the material flow in a perfusion bioreactor.

In this study, using a CFD model, the effects of critical scaffold parameters (such as the number of scaffolds, scaffold diameter, scaffold thickness, and number of pores) on the main flow properties (i.e., flow pressure, wall shear stress, and streamline velocity) influential in cell proliferation and bone development will be investigated. It was observed that increasing the number of pores, in addition to decreasing the pore diameter had an adverse effect on the maximum forces occurring on the scaffold. In addition, changing the overall scaffold diameter did not appear to have as much as an effect as the other parameters. Furthermore, it was observed that a decrease in porosity would lead to an increase in wall shear stress and consequently in cell death. Overall, the outcomes of this study pave the way for optimal design, fabrication, and preparation of cell-laden bone scaffolds for treatment of bone fractures in clinical settings.

Keywords: Advanced manufacturing; computational fluid dynamics (CFD); bioreactors; bone tissue engineering.

* Contact author. Tel.: +1(315)395-4598; fax: +1(304)696-5454; e-mail address: salary@marshall.edu.

1. INTRODUCTION

1.1. Goal and Objectives

In the field of tissue engineering, scaffolds are used to help promote total cellular regeneration in affected areas that receive a deformation of some sort [1, 2]. These deformations differ in terms of severity; for example, they could be tears in a muscle, cuts in tissue, and even fractures in a bone. In terms of a severe deformation in the tissue, a medical practitioner might decide that adding a traditional implant would not be in the patient's best interest, and instead decide to use a scaffold to promote cellular regeneration of the surrounding tissue. In order to achieve this result, an instrument known as a scaffold is used. Similar to traditional scaffolding, the main function of this type is to support the cells by creating an environment that allows them to interact and divide.

The primary step in using these scaffolds is to create a proficient geometry. Once it has been created and undergone mechanical property testing, biological testing is the next step [3, 4]. To do this the use of bioreactors are utilized. Bioreactors provide an environment beneficial for cells to divide and grow, with the end goal to be placed within a living specimen with little to no adverse reactions. There are four main types of bioreactors: (i) rotating wall, (ii) spinner flask, (iii) compression, and (iv) perfusion bioreactor [5]. The type of bioreactor this study focuses on is perfusion bioreactors. Within this type of bioreactor there are two subsections, with the first type being known as an indirect perfusion bioreactor. For indirect perfusion bioreactors, the scaffold is either free floating in the bioreactor or suspended in the middle with the use of other materials, allowing the flow to go around the scaffold [5]. The other perfusion bioreactor is known as direct flow. As the name suggests, the scaffold is snug against the wall of the bioreactor, causing the flow to have contact with the scaffold instead of allowing the flow around it,

as is the case with the previous type [6]. For the simulations conducted in this study, a direct perfusion bioreactor was used.

Direct perfusion bioreactors were determined to be the most beneficial for these simulations due to the disadvantages of the other bioreactor types. Since bone tissue scaffolding have intricate geometries, both rotating wall and spinner flask were found to be ineffective for the tissue scaffolding due to possibly providing an inconsistent distribution of cells within the inner portion of the geometry. As a result, perfusion bioreactors were chosen as they provide a consistent flow of fluid through the entirety of the tissue scaffolding. However, bioreactors are not the only factor that contribute to a successful cell seeding, the other being the tissue scaffold geometry. If the scaffold geometry does not provide adequate interconnections for cells to interact with one another, as well as areas of low cell death, there is a high probability that the cell seeding would be unsuitable for cell proliferation. Therefore, the main goal of this study was to determine the effects critical variable parameters of a scaffold geometry that can have on a bone scaffold's success rate after cell seeding has occurred.

1.2. Review of Literature

Within a review of literature, it was found that many did not focus on researching the optimization of current bone scaffold geometry. In fact, in the case with Grayson *et al*., while they did research the critical variable parameter flow velocity, they used a decellularized bone tissue scaffold [7]. As a result, they did not focus on the scaffold geometry since it was already known to support cell viability [8]. In fact, their results actually concluded that there were other critical parameters that had more impact towards scaffold success rate.

A study conducted by Felder *et al*. also focused on optimizing the flow rate within a perfusion bioreactor [9]. However, unlike the previous study, they used a scaffold that consisted of fibers, making the geometry random and difficult to simulate.

In another conducted study, while Clark *et al*. simulated changes in scaffold pore geometry, they maintained the same porosity by only changing one critical parameter, resulting in some of the scaffolding geometry having greater empty space [10]. When dealing with cells, it is important to provide space for them to proliferate and differentiate, while also preventing large gaps that limit interaction. This idea is mentioned in a different study by Gaspar *et al*. as being an important component when dealing with perfusion bioreactors [11].

Focusing on the bioreactor portion, a study conducted by Kang *et al*. noticed that the spinner flask bioreactors, while easier to use, resulted in undesired structures within the scaffold itself found that a form of perfusion reactor got rid of this problem [12].

In a study conducted by Yan *et al*., a scaffold consisting of a lattice type geometry was used with the variable parameters being the diameter of each strand as well as the distance between each strand changing [13].

However, comparing the focus and results of each piece of literature, there is a noticeable gap in regards to the effects the geometry of a scaffold could have when placed in a perfusion bioreactor. This study aims to focus on these critical variable parameters in scaffold geometry as well as their effects on possible cell viability.

2. MATERIAL AND METHODS

2.1. Materials

This section will focus on describing the methods used for the scaffold and bioreactor geometry, meshing, fluid properties, boundary conditions and governing equations, and numerical solutions used for each simulation. Each of the simulations were completed entirely within the Ansys (Fluent) simulation software.

2.2. Computational Fluid Dynamics (CFD)

2.2.1. Scaffold and Bioreactor Design

The default geometry of the bone scaffold simulated consisted of a simple cylindrical solid of 3 mm in diameter with a height of 1 mm. There were also 5 pores along the surface, located at the center as wells as the four cardinal directions; the diameter of the pores consisted of 0.5 mm. To create this geometry with these specifications, Ansys Design Modeler in the Ansys system Fluid Flow (Fluent) was used. For the perfusion bioreactor, a simple geometry of a cylinder was used. The dimensions consisted of a diameter of 3 mm with a length of 30 mm. Within Design Modeler, the add frozen option was used, resulting in the bioreactor to become the fluid domain with the scaffold being a solid figure. The resulting default geometry of the scaffold and the bioreactor domain can be seen in Figure 1.

For the simulations presented in this study, the main focus is to observe fluid interactions as a function of consequential scaffold and bioreactor geometry parameters. The material of the scaffolds is kept consistent and is not included in the modeling as a variable. In general material and material-related factors, such as surface roughness, affect the formation of boundary layers, adhesion and wetting properties (including hydrophobicity/hydrophilicity and contact angle), conductivity, and ultimately the dynamics of material transport in bioreactors.

2.2.2. Meshing

Meshing is an important component of computational fluid dynamic simulations. The meshing used for these simulations consisted of the pre-generated meshing developed within Ansys Fluent on both the scaffold and bioreactor domain. Viewing the generated mesh, there was a clear definition between the scaffold geometry and the fluid domain. When checking the aspect ratio, which is defined as the surface area in relation to the thickness of the matrix, it was found that each mesh was within an acceptable range [14]. This aspect ratio is used to determine the quality of the meshing domain which contributes to accurate analysis of fluid phenomena.

2.2.3. Fluid Properties

For the fluid used for these simulations, the properties of a cell media was used instead of water. However, unlike practical applications, there were no cells within the media since the focus

was to determine if the fluid interactions with different scaffold parameters could possibly kill any cells within the fluid. Note that the type of cells (such as osteoblast cells used for bone tissue engineering) can significantly affect the flow properties of biological fluids, particularly viscosity, due to their unique physical and biological characteristics. In addition, it has been observed that biological factors such as cell size and shape, cell concentration, cell flexibility and deformability, and cell surface properties are consequential factors affecting the dynamics of the fluid flow in a perfusion bioreactor and thus the rate of cell proliferation and differentiation.

There are many different types of cell media on the market, each with their own properties. For this study, the cell media used was RPMI-1640. This media has a density of 999.3 kg/m^3 and a viscosity of 0.733 x 10^{-3} kg/m.s [15]. These fluid properties were then applied within Ansys as the fluid material.

2.2.4. Boundary Conditions & Governing Equations

To determine if a flow within a simulation will act laminar or in a transitional flow approaching turbulent path-lines, the Reynolds number equation will give insight into this fluid motion. Thus, equation (1) shown below is used [16].

$$Re = \frac{\rho u L}{\mu} \quad (1)$$

The variables used in this equation are density (ρ) in kg/m^3, flow velocity (u) in m/s, length of the geometry (L) in m, and the dynamic viscosity (μ) in kg/m.s. This results in a nondimensionalized number that allows for a flow to be categorized as laminar, turbulent, or in a transition stage. In regards to these simulations, the Reynold's number was calculated for each simulation using equation (1). It was found that for a circular pipe, which is the general form of the bioreactor, the Reynold's number was within the laminar range, resulting in the methods used in Ansys to be laminar.

In order to successfully use a perfusion bioreactor, there are multiple parts aside from itself. A pump is used to induce the consistent flow needed for this bioreactor type; hence, there is a defined inlet velocity needed. According to literature, there is a wide range of inlet velocities that could be used, however, a smaller inlet velocity of 4.7152 mm/s was used in this case [17]. This velocity was then placed on the top surface of the bioreactor geometry, with a pressure outlet along the bottom surface of the bioreactor. The circular walls consisted of a stationary wall as well as the scaffold geometry being a separate wall. This can be viewed in Figure 1. Finally, for all simulations performed, a linearization tolerance of 1E-6 was set for all conservation imbalances in order to obtain an accurate steady-state solution.

Thus, with the conclusion of the fluid being laminar the Navier-Stokes equation for the fully developed flow will be used [18, 19].

$$\rho \frac{\partial u}{\partial t} - \mu \nabla^2 u + \rho(u\nabla)u + \nabla p = F \quad (2)$$

As shown in the equation above, the density (ρ) in kg/m^3, flow velocity (u) in m/s, and dynamic viscosity (μ) in kg/m.s are used.

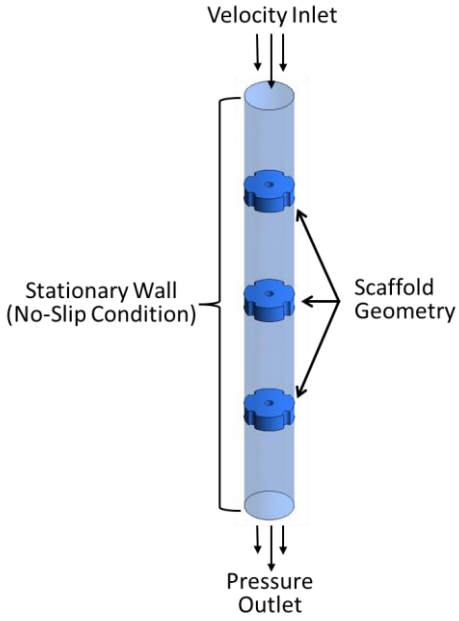

Figure 1: Boundary conditions of the CFD model.

2.2.5. Numerical Solutions

To run the simulations, a Coupled Scheme was used as well as the Least squared Cell Based gradient. The Pressure and Momentum were set to Second Order and Second Order Upwind, respectively. The time method for these simulations were set to a Global Time Step. For the amount of simulation iterations, a total of 10,000 was used to allow the results to converge and stabilize. However, the majority of the simulations converged before it reached the 300 iteration mark.

This study focused on multiple different variables of scaffold geometries. These variables consisted of: the overall scaffold diameter, scaffold height, number of pores, diameter of the pores, number of scaffolds, as well as the distance between two scaffolds. The list of variables with the values recorded can be viewed in Table 1. The reason for viewing different variables is due to differences in scaffold designs. Each scaffold is created with a specific function in mind; for bone scaffolds, the geometry of the scaffold has to provide enough support to be placed near or in original bone tissue. The geometry must also support the cells that would be placed onto the scaffold within the bioreactor. Hence, there are many variables that must be considered. As the simulations provided by this study can show, simply changing one variable can determine whether the scaffold can successfully support cells or not.

Table 1: List of parameters of critical scaffold variations. Note that the cells in black are the default variables.

Simulation Iterations	Scaffold Diameter [mm]	Scaffold Thickness [mm]	Number of Pores	Pore Diameter [mm]	Number of Scaffolds	Distance Between Two Scaffolds [mm]	Length of the Bioreactor (Domain) [mm]
1.1	3	1	5	0.5	1	7	30
1.2	5	1	5	0.5	1	7	30
1.3	9	1	5	0.5	1	7	30
2.1	3	1	5	0.5	1	7	30
2.2	3	5	5	0.5	1	7	30
2.3	3	10	5	0.5	1	7	30
2.4	3	15	5	0.5	1	7	30
3.1	3	1	5	0.5	1	7	30
3.2	3	1	7	0.5	1	7	30
3.3	3	1	9	0.5	1	7	30
3.4	3	1	13	0.5	1	7	30
4.1	3	1	5	0.5	1	7	30
4.2	3	1	5	0.25	1	7	30
4.3	3	1	5	0.2	1	7	30
4.4	3	1	5	0.1	1	7	30
5.1	3	1	5	0.5	1	7	30
5.2	3	1	5	0.5	2	7	30
5.3	3	1	5	0.5	3	7	30
5.4	3	1	5	0.5	4	7	30
6.1	3	1	5	0.5	2	1	30
6.2	3	1	5	0.5	2	3	30
6.3	3	1	5	0.5	2	5	30
6.4	3	1	5	0.5	2	7	30
6.5	3	1	5	0.5	2	10	30

3. RESULTS AND DISCUSSION

The interactions between the scaffold and the media have an important role in a scaffold's success. In practical applications, the media that flows through the bioreactor would contain cells, as the main function of a bioreactor is to provide an environment for cells to proliferate. Due to this, it is important to understand the interaction between the scaffold and fluid in terms of velocity, pressure, and wall shear stress (WSS). It has been found in research papers that the cells used for bone scaffolds are extremely susceptible to shear stress [20]. In fact, WSS is capable of inducing cell differentiation at nearly any range; however, if the WSS is above 60 mPa, any cells that would be present in the media would die after coming into contact with that area of the geometry [21]. In regards to velocity, cells can undergo a decent amount. For example, blood cells in the human body can be expected to be under a velocity ranging from 0.15-0.49 m/s without the cells dying [22]. Each fluid interaction is used to determine if the changes in critical scaffold parameters have a detrimental effect on scaffold success, as is discussed below.

3.1. Scaffold Diameter

When comparing the results of the fluid properties while the overall scaffold diameter is changing, there is no obvious difference between the maximum velocity, pressure, and WSS. However, a slight decrease in pressure and WSS can be seen as the scaffold diameter increases, as shown in Figure 2(b) and Figure 2(c), respectively. Viewing the WSS values illustrated in Figure 2(c), it is clear that by increasing the scaffold diameter, there would be little, if any, cellular death occurring along the scaffold. It can also be said that changing the scaffold diameter to 9 mm will not have a significant impact on the fluid interactions.

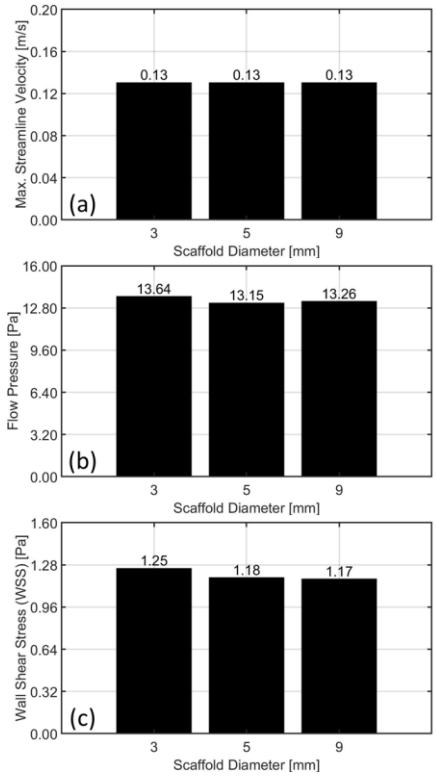

Figure 2: Maximum values of (a) velocity, (b) pressure, and (c) WSS as the diameter of the scaffold increases.

Figure 3 exhibits the influence of the scaffold diameter on streamline velocity, flow pressure, and WSS. When examining the streamline velocity, the maximum velocity can be found as the flow goes through each pore, with the center pore having the highest value. This action can be attributed to the pores acting as a nozzle, as shown by the streamline attributes once exiting the pores. Comparing the pressure contour plots, shown in Figure 3(a-ii), (b-ii), and (c-ii), they are similar between the scaffold diameter variables, with the maximum value being found along the top surface of the scaffold. There is also a decrease in pressure along the sides of the top surface of the scaffold, as well as within the pores, with the sides of the scaffold that interact with the bioreactor having the minimum pressure due to the scaffold being snug against the bioreactor. Viewing the WSS contour plots, illustrated in Figure 3(a-iii), (b-iii), and (c-iii), the distribution of WSS values is similar except for differences in values, as was the case with pressure. The minimum WSS could be found all along the scaffold with the only changes being found as an increase in WSS along the pores. The maximum WSS

could be found along the walls of the inner pore, further suggesting that the inner pore acts as a nozzle.

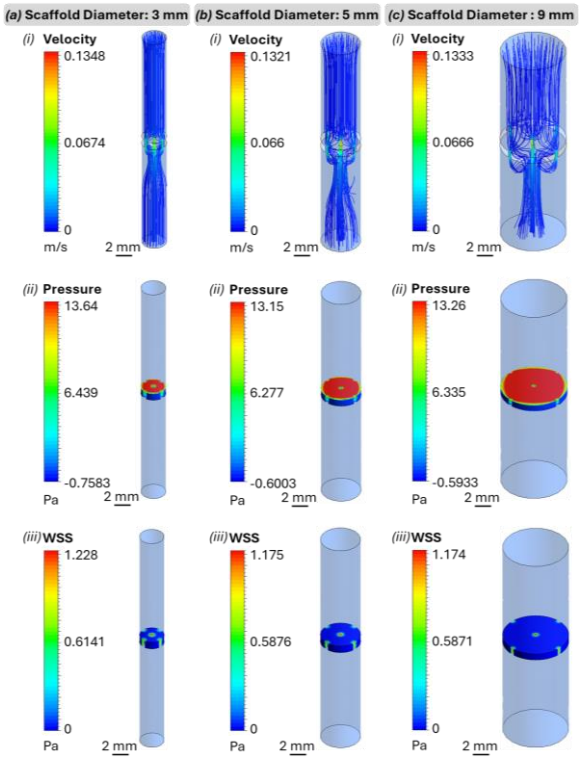

Figure 3: Maximum values of streamline velocity, pressure, and WSS as a function of the Scaffold Diameter: (a) 3 mm, (b) 5 mm, and (c) 9 mm.

3.2. Scaffold Thickness

When comparing the increase in scaffold thickness, there is a definite increase in maximum pressure which is visible in Figure 4(b). This begins to be visible after the scaffold is increased to 5 mm, where the pressure continues to linearly increase with the scaffold thickness. There is also a slight increase in maximum velocity and WSS that appears to flatten out, as illustrated in Figure 4(b) and Figure 4(c) respectively. Even with this slight increase, the maximum WSS and streamline velocity values are not near the range previously stated that can kill cells; however, it still remains that changing the thickness of the scaffold can drastically affect the pressure that occurs on said scaffold.

As indicated in Figure 5(a-i)-(d-i), the streamline velocity shows that the inner pore acts as a nozzle, regardless of the scaffold thickness. However, when viewing the pressure contour plot, there is a difference between the scaffold thicknesses; comparing Figure 5(d-ii) and Figure 5(a-ii), the pressure along the outer pores is different. It appears that as the scaffold thickness increases, the maximum pressure can also be found along the top of these pores instead of only on the top surface of the scaffold. Another difference is the pressure along these outer pores also appears to decrease as the flow continues through the pore. Despite these differences, there are still similarities between the four scaffold thickness variables, as shown in Figure 5(a-iii)-(d-iii). For example, the WSS contour plot distribution is the same with only the variables being different.

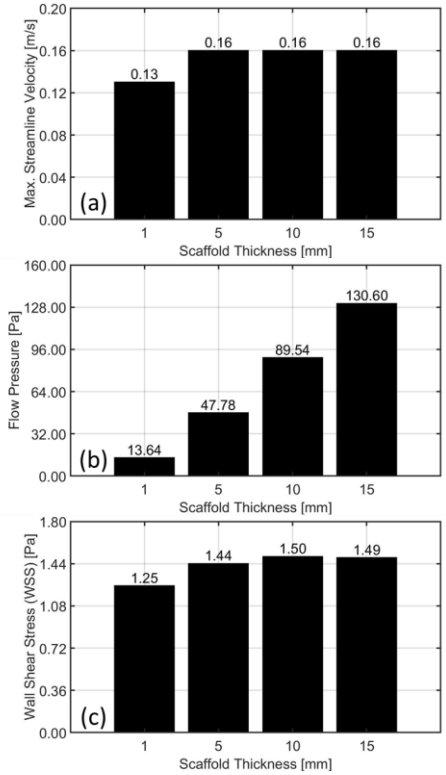

Figure 4: Maximum values of (a) velocity, (b) pressure, and (c) WSS as the overall thickness of the scaffold increases.

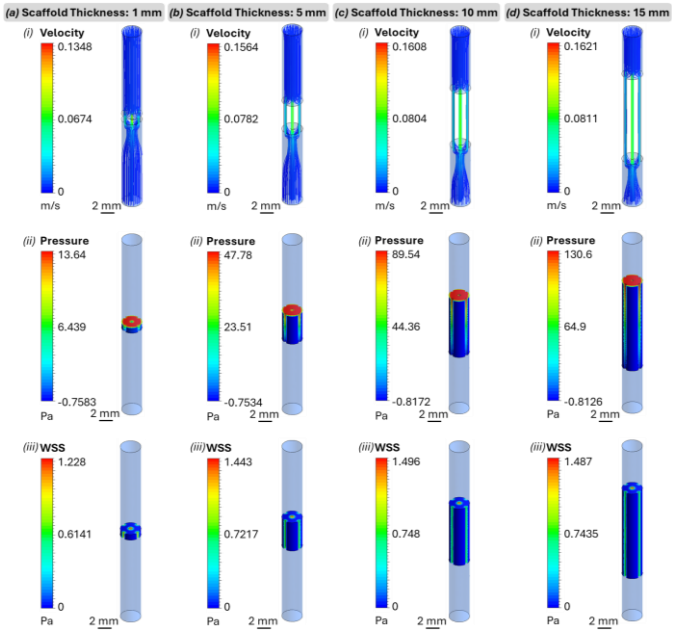

Figure 5: Maximum values of streamline velocity, pressure, and WSS as a function of the Scaffold Thickness: (a) 1 mm, (b) 5 mm, (c) 10 mm, and (d) 15 mm.

3.3. Number of Pores

As the number of pores increases, the overall porosity of the scaffolds increases. Hence, the maximum velocity, pressure, and WSS are dramatically decreased due to the changes in pore amount. However, there is not as dramatic of a decrease in these response variables between 9 and 13 pores, with the largest decrease being between 5 and any other number of pores, as can be observed in Figure 6.

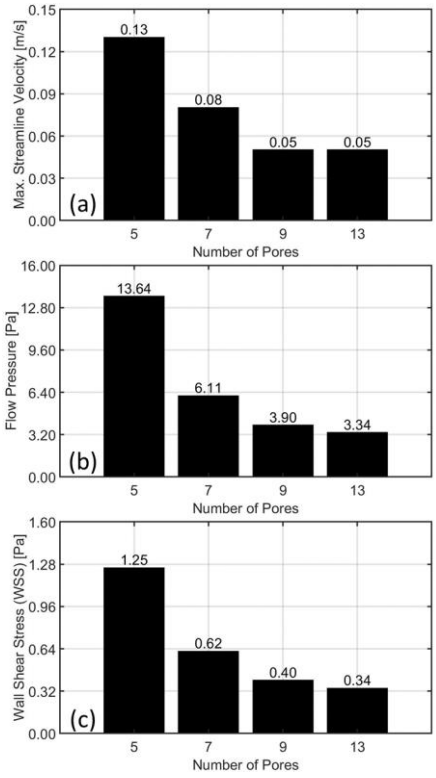

Figure 6: Maximum values of (a) velocity, (b) pressure, and (c) WSS as a function of the number of pores.

As illustrated in Figure 7(a-i)-(d-i), the inner pore acts as a nozzle. However, when the number of pores increases, there are more areas for the flow to go through, decreasing the overall velocity occurring at this middle nozzle-like pore. In regards to the pressure and WSS contour plots shown in Figure 7(a-ii)-(d-ii) and Figure 7(a-iii)-(d-iii) respectively, it is noticed that when a pore is added to the scaffold the distribution of pressure and WSS around one pore remains similar (unlike their magnitude) and is simply exerted to the scaffold. For example, when comparing Figure 7(a-ii) and Figure 7(d-ii), it is observed that: **(i)** the maximum pressure is still found on the top surface of the scaffold, **(ii)** a decrease in pressure is still along the sides of the top surface and along the walls of the pores, **(iii)** and the minimum pressure is found on the walls of the scaffold.

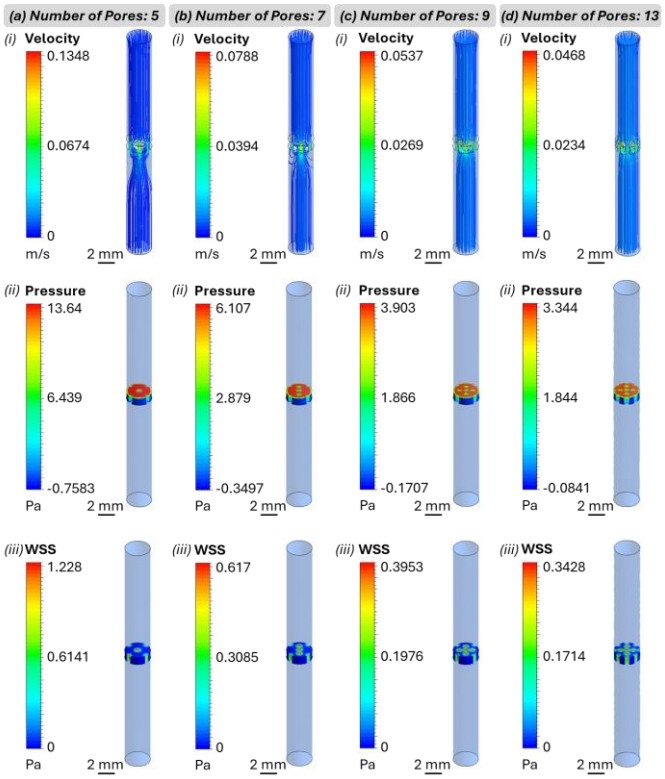

Figure 7: Maximum values of streamline velocity, pressure, and WSS as a function of the number of pores: (a) 5 pores, (b) 7 pores, (c) 9 pores, and (d) 13 pores.

3.4. Pore Diameter

Compared to the previous section, decreasing the pore diameter will in turn decrease the porosity of the scaffold. Therefore, the effects of decreasing the porosity can be visible in these simulation results, as shown in Figure 8. There was a dramatic increase in maximum velocity, pressure, and WSS between all of the simulations, however the most dramatic increase is when the pore diameters are set to 0.1 mm, where the maximum values are significantly different than the other simulation results. Viewing the WSS at this pore diameter, Figure 8(c), the results show it is greater than 200 Pa, due to the ranges of cellular death previously mentioned, it is clear that any cells present would die, resulting in an unsuccessful scaffold.

When viewing the velocity streamlines shown in Figure 9(a-i)-(d-i), it is clear that decreasing the pore diameter has an effect on how the fluid interacts with the scaffold. Comparing the streamlines with each other, it is noticeable that the flow becomes more erratic as the diameter decreases (as implied from Figure 9(a-i)). Comparing the pressure and WSS contour plots illustrated in Figure 9(a-ii)-(d-ii) and Figure 9(a-iii)-(d-iii) respectively, in regards to the areas where the maximum and minimum values can be found on the scaffold, there are no noticeable changes.

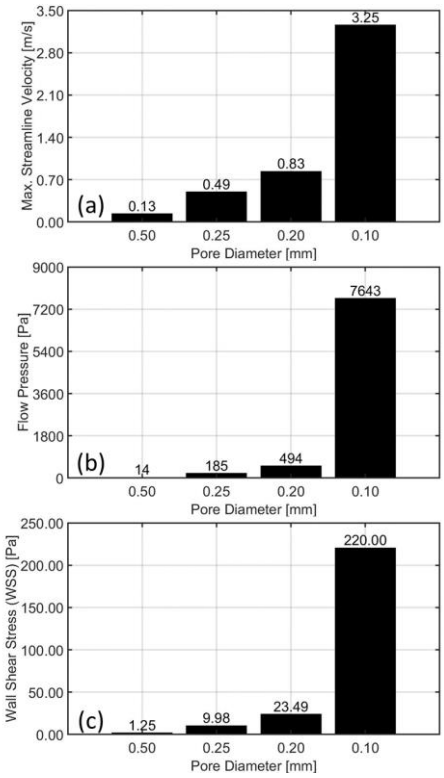

Figure 8: Maximum values of (a) velocity, (b) pressure, and (c) WSS as the diameter of the pores on the scaffold decrease.

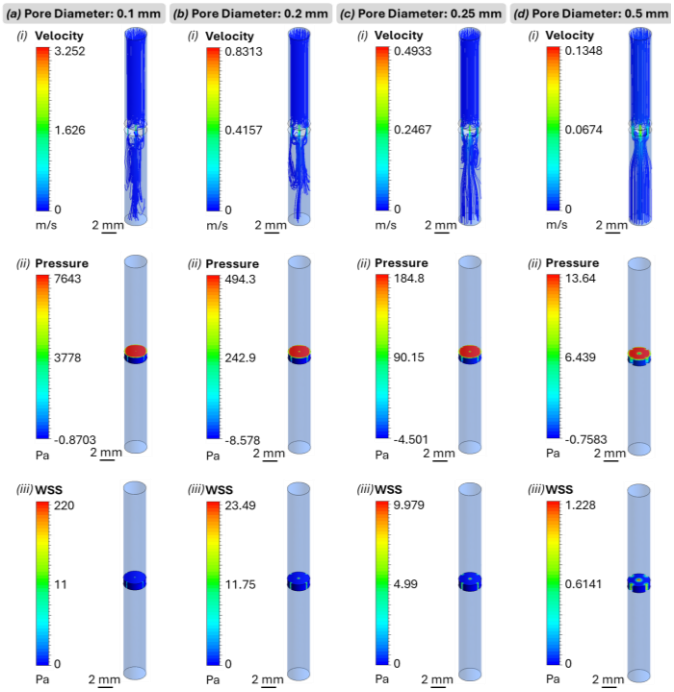

Figure 9: Maximum values of streamline velocity, pressure, and WSS as a function of the Pore Diameter: (a) 0.50 mm, (b) 0.25 mm, (c) 0.20 mm, and (d) 0.10 mm.

3.5. Number of Scaffolds

Implied from Figure 10(a) and Figure 10(b), when increasing the number of scaffolds while maintaining the same amount of spacing between them, there appears to be an increase in maximum pressure as well as maximum velocity, both having an increasing linear trend. However, in regards to WSS, as shown in Figure 10(c), there does not appear to be any specific trend between the increasing number of scaffolds. Even with there being no consistent trend, the maximum WSS for each simulation is still below the cellular death range, resulting in these parameters theoretically producing successful scaffolds.

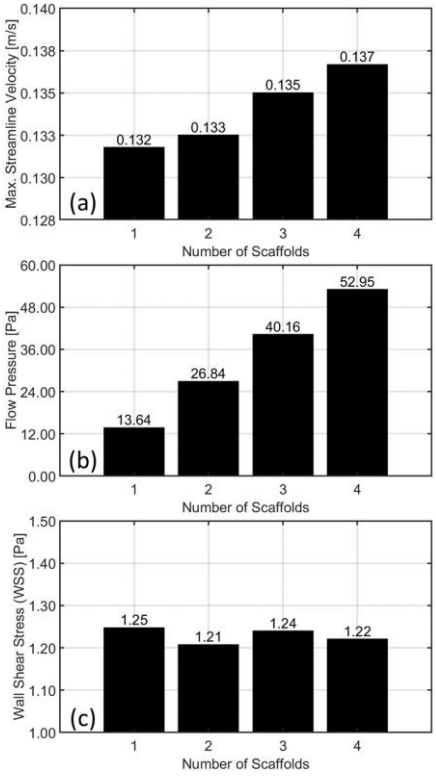

Figure 10: Maximum values of (a) velocity, (b) pressure, and (c) WSS as the number of scaffolds increase.

When viewing the velocity streamlines shown in Figure 11(a-i)-(d-i), even with increasing the number of scaffolds, the middle pore on each scaffold still acts as the primary pore for material transport (having a full-circle, open geometry compared to the semi-circle/semi-open geometry of the other pores) in each simulation, with the only noticeable difference being a decrease in streamline density as the scaffold number increases. In regards to the pressure occurring on each scaffold, illustrated in Figure 11(a-ii)-(d-ii), it appears that only the top scaffold, or the one that interacts with the fluid first, will have the maximum pressure along the top surface, with the pressure decreasing as it reaches the next scaffold. This implies that the first scaffold (referred to as the sacrifice scaffold) would not result in positive cell proliferation. For the WSS occurring on the scaffolds, illustrated in Figure 11(b-iii) and Figure 11(d-iii), it similarly appears that only the top scaffold undergoes a high level of wall shear stress

(leading to cell death). However, as shown in Figure 11(c-iii), it appears that the middle scaffold seems to undergo the same WSS as the top scaffold (in regards to the contour plot).

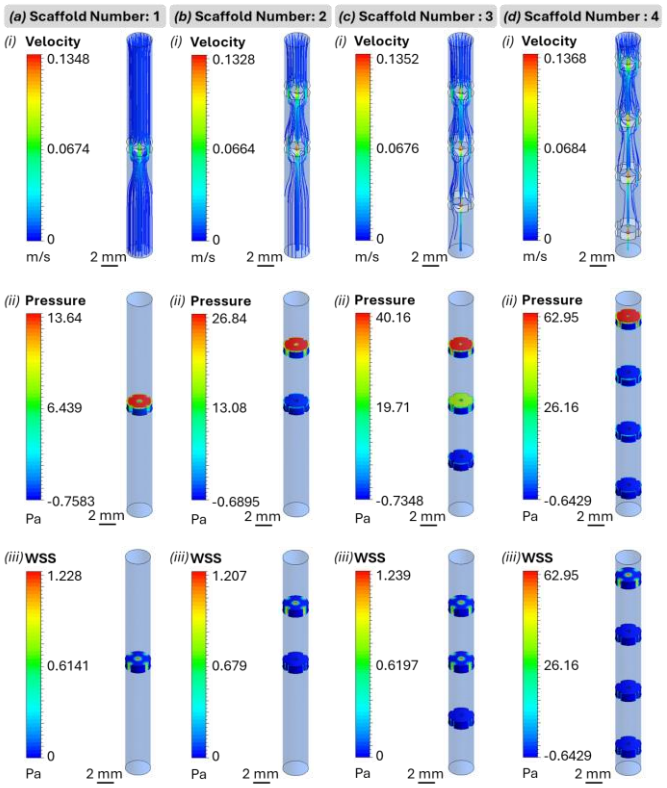

Figure 11: Maximum values of streamline velocity, pressure, and WSS as a function of the number of scaffolds: (a) 1 scaffold, (b) 2 scaffolds, (c) 3 scaffolds, and (d) 4 scaffolds.

3.6. Distance Between Two Scaffolds

Comparing the maximum velocity when changing the distance between two scaffolds, there is a decrease in the velocity as the distance increases. However, as shown in Figure 12(a), when the distance is 10 mm the velocity increases slightly. This can also be said for the maximum WSS. As the distance increases, the maximum WSS also decreases, except for when the distance is 10 mm, as shown in Figure 12(c). For maximum pressure, Figure 12(b), the graph appears to flatten out after the distance reaches 5 mm, with there being slight variations between 5 mm, 7 mm, and 10 mm; however, each maximum value is still within the ranges cells can withstand.

When viewing the velocity streamlines shown in Figure 13(a-i)-(e-i), when the distance between the two scaffolds are 3 mm and 5 mm there appears to be some erratic motion in between the two scaffolds. However, when the distance is decreased to 1 mm, the flow appears to go directly through the pores of each scaffold, causing there to be no erratic motion between the two scaffolds. Similar to the previous section, the pressure contour plots shown in Figure 13(a-ii)-(d-ii) show that the top scaffold receives the maximum pressure while the bottom scaffold receives less pressure.

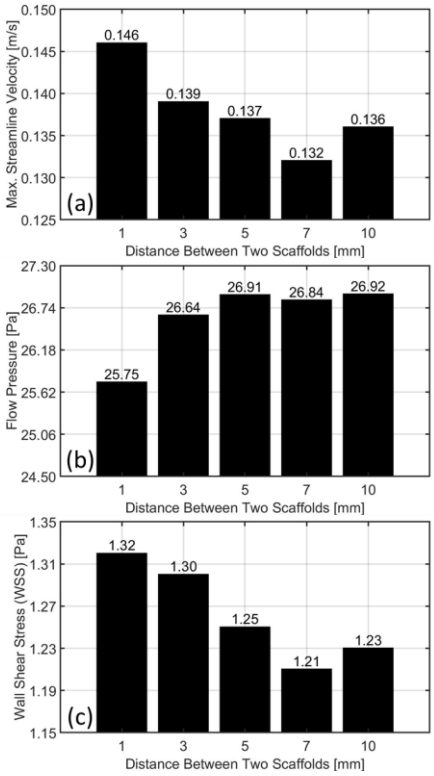

Figure 12: Maximum values of (a) velocity, (b) pressure, and (c) WSS as the distance between scaffolds increases.

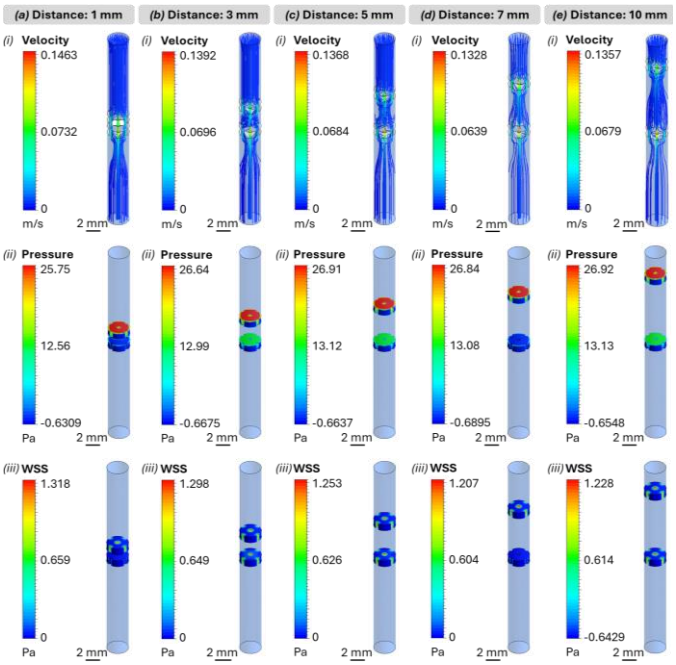

Figure 13: Maximum values of streamline velocity, pressure, and WSS as a function of the distance between two scaffolds: (a) 1 mm, (b) 3 mm, (c) 5 mm, (d) 7 mm, and (e) 10 mm.

For the WSS contour plots, both scaffolds appear to undergo the same WSS as shown in Figure 13(b-iii), (c-iii), and (e-iii). Despite this, when the distance between the two scaffolds are 1 mm and 7 mm the two scaffolds do not withstand the same WSS, with the majority of the bottom scaffold undergoing the minimum value.

4. CONCLUSIONS AND FUTURE WORK

4.1. Conclusions

The primary objective of these simulations was to study the interactions between different critical variation parameters of scaffold geometries used in tissue engineering. The secondary objective was to determine if it was possible to include multiple scaffolds within a single perfusion bioreactor. The overall goal being to determine if it is possible to decrease the amount of waste and overall cost needed to run cell seeding procedures in a practical application. It was found that changing the porosity, either by increasing the number of pores or decreasing the pore diameter, had a dramatic effect on the maximum forces occurring on the scaffold. Changing the overall scaffold diameter did not appear to have as much of an effect as the other parameters. Of all of the simulations, there was only one that would theoretically result in the failure of the scaffold due to cellular death, that parameter being a significant decrease in porosity. However, there are many practical aspects that would have to be taken into consideration to truly determine if the scaffold was successful. For example, deformations in the scaffold geometry during printing, contamination of cells or media, and even mechanical problems of critical devices are all potential issues to keep in mind.

4.2. Future Work

Future work consists of changing the bone scaffold geometry to a more complex form. This would consist of a triply periodic minimal surface (TPMS) geometry that would be produced into an overall cylindrical form suited for analysis of perfusion bioreactors. The simulations would be conducted in a similar manner in regard to the methods developed in this study.

ACKNOWLEDGMENTS

Dr. Salary would like to thank the National Science Foundation (NSF) for funding this work under award # *OIA-2327460*.

REFERENCE

[1] Lawrence, L. M., Salary, R., Miller, V., Valluri, A., Denning, K. L., Case-Perry, S., Abdelgaber, K., Smith, S., Claudio, P. P., and Day, J. B., 2023, "Osteoregenerative Potential of 3D-Printed Poly ε-Caprolactone Tissue Scaffolds In Vitro Using Minimally Manipulative Expansion of Primary Human Bone Marrow Stem Cells," International Journal of Molecular Sciences, 24(5), p. 4940, DOI: 10.3390/ijms24054940.

[2] Salary, R., 2022, "Perspective Chapter: Advanced Manufacturing for Bone Tissue Engineering and Regenerative Medicine," Advanced Additive Manufacturing, I. V. Shishkovsky, ed., IntechOpen, London, UK, p. 59, DOI: 10.5772/intechopen.102563.

[3] Yu, M., Yeow, Y. J., Lawrence, L., Claudio, P. P., Day, J. B., and Salary, R., 2021, "Characterization of the Functional Properties of PCL Bone Scaffolds Fabricated Using Pneumatic Microextrusion " Journal of Micro-and Nano-Manufacturing, JMNM-20-1074, DOI: 10.1115/1.4051631.

[4] Abdelgaber, Y., Klemstine, C., and Salary, R., 2023, "A Novel, Image-Based Method for Characterization of the Porosity of Additively Manufactured Bone Scaffolds With Complex Microstructures," Journal of Manufacturing Science and Engineering, 145(4), p. 041008, DOI: 10.1115/1.4056434.

[5] Burova, I., Wall, I., and Shipley, R. J., 2019, "Mathematical and Computational Models for Bone Tissue Engineering in Bioreactor Systems," Journal of tissue engineering, 10, p. 2041731419827922, DOI: 10.1177/20417314198279.

[6] Sladkova, M., and De Peppo, G. M., 2014, "Bioreactor Systems for Human Bone Tissue Engineering," Processes, 2(2), pp. 494-525, DOI: 10.3390/pr2020494.

[7] Grayson, W. L., Marolt, D., Bhumiratana, S., Fröhlich, M., Guo, X. E., and Vunjak-Novakovic, G., 2011, "Optimizing the Medium Perfusion Rate in Bone Tissue Engineering Bioreactors," Biotechnology and bioengineering, 108(5), pp. 1159-1170, DOI: 10.1002/bit.23024.

[8] Ma, C. Y. J., Kumar, R., Xu, X. Y., and Mantalaris, A., 2007, "A Combined Fluid Dynamics, Mass Transport and Cell Growth Model for a Three-Dimensional Perfused Biorector for Tissue Engineering of Haematopoietic Cells," Biochemical engineering journal, 35(1), pp. 1-11, DOI: 10.1016/j.bej.2006.11.024.

[9] Felder, M. L., Simmons, A. D., Shambaugh, R. L., and Sikavitsas, V. I., 2020, "Effects of Flow Rate on Mesenchymal Stem Cell Oxygen Consumption Rates in 3D Bone-Tissue-Engineered Constructs Cultured in Perfusion Bioreactor Systems," Fluids, 5(1), p. 30, DOI: 10.3390/fluids5010030.

[10] Clark, S., Quigley, C., Mankowsky, J., and Habib, A., "A Simulation Approach to Determine Internal Architecture of 3D Bio-Printed Scaffold Suitable for A Perfusion Bioreactor," Proc. IIE Annual Conference. Proceedings, Institute of Industrial and Systems Engineers (IISE), pp. 1-6, DOI: 10.21872/2023IISE_2255.

[11] Gaspar, D. A., Gomide, V., and Monteiro, F. J., 2012, "The Role of Perfusion Bioreactors in Bone Tissue Engineering," Biomatter, 2(4), pp. 167-175, DOI: 10.4161/biom.22170.

[12] Kang, C. W., Wang, Y., Tania, M., Zhou, H., Gao, Y., Ba, T., Tan, G. D. S., Kim, S., and Leo, H. L., 2013, "Computational Fluid Modeling and Performance Analysis of a Bidirectional Rotating Perfusion Culture System," Biotechnology Progress, 29(4), pp. 1002-1012, DOI: 10.1002/btpr.1736.

[13] Yan, X., Chen, X., and Bergstrom, D., 2011, "Modeling of the Flow within Scaffolds in Perfusion Bioreactors," Am J Biomed Eng, 1(2), pp. 72-77, DOI: 10.5923/j.ajbe.20110102.13.

[14] Lawrence, B. J., Devarapalli, M., and Madihally, S. V., 2009, "Flow Dynamics in Bioreactors Containing Tissue Engineering Scaffolds," Biotechnology and bioengineering, 102(3), pp. 935-947, DOI: 10.1002/bit.22106.

[15] Poon, C., 2022, "Measuring the Density and Viscosity of Culture Media for Optimized Computational Fluid Dynamics Analysis of *in vitro* Devices," Journal of the mechanical behavior of biomedical materials, 126, p. 105024, DOI: 10.1016/j.jmbbm.2021.105024.

[16] Huang, Z., Odeleye, A. O. O., Ye, H., Cui, Z., and Yang, A., 2018, "Fluid Dynamic Characterization of a Fluidized-Bed Perfusion Bioreactor with CFD–DEM Simulation," Journal of Chemical Technology & Biotechnology, 93(8), pp. 2316-2330, DOI: 10.1002/jctb.5576.

[17] Zhao, F., van Rietbergen, B., Ito, K., and Hofmann, S., 2018, "Flow Rates in Perfusion Bioreactors to Maximise Mineralisation in Bone Tissue Engineering *in vitro*," Journal of Biomechanics, 79, pp. 232-237, DOI: 10.1016/j.jbiomech.2018.08.004.

[18] Salary, R., Lombardi, J. P., Weerawarne, D. L., Rao, P., and Poliks, M. D., 2021, "A Computational Fluid Dynamics Investigation of Pneumatic Atomization, Aerosol Transport, and Deposition in Aerosol Jet Printing Process," Journal of Micro-and Nano-Manufacturing, 9(1), p. 010903, DOI: 10.1115/1.4049958.

[19] Salary, R., Lombardi, J. P., Tootooni, M. S., Donovan, R., Rao, P. K., Borgesen, P., and Poliks, M. D., 2017, "Computational Fluid Dynamics Modeling and Online Monitoring of Aerosol Jet Printing Process," Journal of Manufacturing Science and Engineering, 139(2), p. 021015, DOI: 10.1115/1.4034591.

[20] Carpentier, B., Layrolle, P., and Legallais, C., 2011, "Bioreactors for Bone Tissue Engineering," The International journal of artificial organs, 34(3), pp. 259-270, DOI: 10.5301/IJAO.2011.6333.

[21] Omar, A. M., Hassan, M. H., Daskalakis, E., Ates, G., Bright, C. J., Xu, Z., Powell, E. J., Mirihanage, W., and Bartolo, P. J., 2022, "Geometry-Based Computational Fluid Dynamic Model for Predicting the Biological Behavior of Bone Tissue Engineering Scaffolds," Journal of Functional Biomaterials, 13(3), p. 104, DOI: 10.3390/jfb13030104.

[22] Klarhöfer, M., Csapo, B., Balassy, C., Szeles, J., and Moser, E., 2001, "High-Resolution Blood Flow Velocity Measurements in the Human Finger," Magnetic Resonance in Medicine: An Official Journal of the International Society for Magnetic Resonance in Medicine, 45(4), pp. 716-719, DOI: 10.1002/mrm.1096.